UNIVERSITÄT AUGSBURG
Universitätsbibliothek

OPEN ACCESS
OPUS AUGSBURG

Continuous observation of filaments from the confined region to the far scrape-off layer

M. Griener, E. Wolfrum, Gregor Birkenmeier, M. Faitsch, R. Fischer, G. Fuchert, L. Gil, G. F. Harrer, P. Manz, D. Wendler, U. Stroth

Angaben zur Veröffentlichung / Publication details:

Griener, M., E. Wolfrum, Gregor Birkenmeier, M. Faitsch, R. Fischer, G. Fuchert, L. Gil, et al. 2020. "Continuous observation of filaments from the confined region to the far scrape-off layer." *Nuclear Materials and Energy* 25: 100854. https://doi.org/10.1016/j.nme.2020.100854.

Nutzungsbedingungen / Terms of use:

CC BY-NC-ND 4.0

Dieses Dokument wird unter folgenden Bedingungen zur Verfügung gestellt: / This document is made available under these conditions:
CC-BY-NC-ND 4.0: Creative Commons: Namensnennung - Nicht kommerziell - Keine Bearbeitung
Weitere Informationen finden Sie unter: / For more information see:
https://creativecommons.org/licenses/by-nc-nd/4.0/deed.de

Nuclear Materials and Energy 25 (2020) 100854

Contents lists available at ScienceDirect

Nuclear Materials and Energy

journal homepage: www.elsevier.com/locate/nme

Continuous observation of filaments from the confined region to the far scrape-off layer

M. Griener [a,*], E. Wolfrum [a], G. Birkenmeier [a,d], M. Faitsch [a], R. Fischer [a], G. Fuchert [b], L. Gil [c], G.F. Harrer [e], P. Manz [a], D. Wendler [a,d], U. Stroth [a,d], the ASDEX Upgrade Team [1], the EUROfusion MST1 Team [2]

[a] Max Planck Institute for Plasma Physics, Boltzmannstr. 2, 85748 Garching, Germany
[b] Max Planck Institute for Plasma Physics, Wendelsteinstr. 1, 17491 Greifswald, Germany
[c] Instituto de Plasmas e Fusão Nuclear, Instituto Superior Técnico, Universidade de Lisboa, 1049-001 Lisboa, Portugal
[d] Physik Department E28, Technische Universität München, 85748 Garching, Germany
[e] Institute of Applied Physics, TU Wien, Fusion@ÖAW, Wiedner Hauptstr. 8-10, 1040 Vienna, Austria

ARTICLE INFO

Keywords:
Plasma filaments
Scrape-off layer
Convective transport
Quasi-coherent modes
Confinement regimes
ELM free regimes
Helium beam diagnostic

ABSTRACT

The thermal helium beam diagnostic at ASDEX Upgrade can access the whole plasma edge region simultaneously with a high spatiotemporal resolution. Manifold dynamics of plasma edge transport is observed for different plasma confinement regimes, comprising L- and H-mode scenarios with type-I and small ELMs as well as ELM free EDA regimes. The measurements show that the plasma dynamics in the confined region close to the separatrix is often dominated by regular high frequency modes (10–100 kHz), whereas filaments with an intermittent occurrence rate of 0.1–2 kHz dominate in particular the far scrape-off layer (SOL). The comparison among different regimes shows a similar filamentary activity between L-mode and inter-ELM H-mode phases. An increased filamentary activity in H-mode, however, is found for rising densities n/n_{GW}. This is the case for the regime of quasi continuous exhaust (QCE) with three times higher filament velocities compared to a clean inter-ELM H-mode.

1. Introduction

In magnetic confinement fusion, transport processes in the plasma edge region determine the power load onto first wall components. These power loads must be controlled and minimized on the way towards a fusion power plant. Steady-state power flux into the scrape-off layer (SOL) determines the power fall-off length in the near SOL [1]. As here plasma profile gradients are steep, turbulence can be driven locally by these gradients. In the far SOL, however, the gradients are flattened. Here turbulence spreads from the near SOL into this region in the form of convective filaments [2].

The filament size parallel to the field lines might exceed several meters, the size in radial and poloidal direction, i.e. perpendicular to the field lines, is in the range of 0.1-10 cm [3]. The occurrence of filaments is highly intermittent and the relative fluctuation levels of plasma parameters caused by radially outwards propagating filaments typically increases towards the first wall and can exceed 100 % with an auto-correlation time of the bursts in the order of tens of microseconds [3,4]. Filaments reach the far SOL with a rate which ranges from a few hundred Hz up to several kHz [5,6]. The radial velocity further depends on the plasma scenario and ranges from few hundred meters per second in L-mode up to several km/s for ELM filaments [7–9].

Filaments can dominate the transport in the SOL and thus give rise to a significant part of the thermal load to the first wall [10,11]. Filaments might lead to a damage of wall structures by increasing the sputtering rate in next step devices [11]. An increased filamentary activity can contribute to a flattening of upstream profiles which causes an increase of the power decay length λ_q and a widening of the wetted area in the divertor, as shown in the regime of quasi continuous exhaust (QCE) [12].

In this contribution we present the dynamical behavior at the plasma edge for different confinement regimes, comprising L- and H-mode scenarios (type-I, QCE as well as ELM free EDA regimes). A phenomenological overview of the different dynamics is given in

* Corresponding author.
E-mail address: Michael.Griener@ipp.mpg.de (M. Griener).
[1] See author list of "MEYER, H. et al., Nucl. Fusion **59** (2019) 112014".
[2] See author list of "LABIT, B. et al., Nucl. Fusion **59** (2019) 086020".

https://doi.org/10.1016/j.nme.2020.100854
Received 31 July 2020; Received in revised form 20 October 2020; Accepted 17 November 2020
Available online 28 November 2020
2352-1791/© 2020 The Authors. Published by Elsevier Ltd. This is an open access article under the CC BY-NC-ND license (http://creativecommons.org/licenses/by-nc-nd/4.0/).

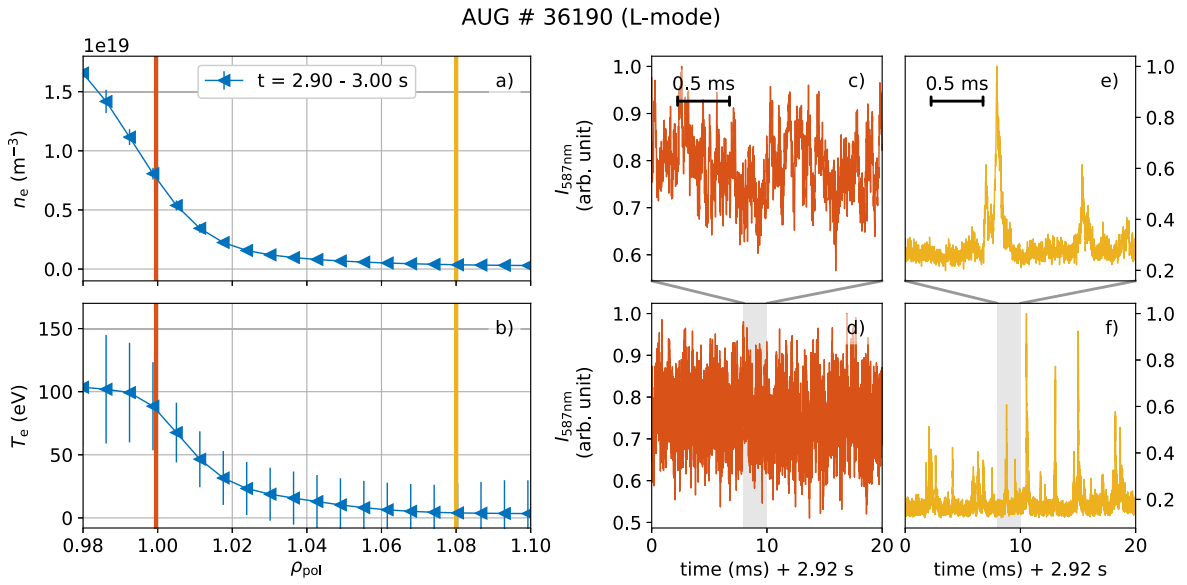

Fig. 1. (a) n_e and (b) T_e plasma profiles for the L-mode discharge # 36 190, evaluated with the THB. Subplots (c) – (f) show the plasma dynamics color-coded at two radial positions at $\rho_{pol} = 1$ and $\rho_{pol} = 1.08$, marked by vertical lines in subplots (a) and (b).

Section 2. In Section 3 we compare filament properties among the regimes presented, focusing on the radial filament velocity, filament occurrence rate and auto-correlation time. Section 4 discusses the importance of filamentary transport and builds a connection of far SOL filaments to the dynamics around the separatrix, which shows the origin of filaments and thus helps to understand the mechanism by which filaments are created.

2. Plasma edge dynamics

In this section we compare different plasma dynamics in the edge region for a variety of confinement regimes at ASDEX Upgrade (AUG). The data are delivered by the thermal helium beam diagnostic (THB) which locally injects a neutral helium cloud into the plasma and monitors the emission of four neutral lines simultaneously [13]. The diagnostic provides a unique coverage of the whole plasma edge region with a high spatiotemporal (3 mm, 900 kHz) resolution. Whereas the line ratio technique [14,15] delivers electron density (n_e) and temperature (T_e) profiles, the direct investigation of the emission change of one neutral helium line can be used to investigate turbulent structures, comparable to the gas puff imaging techniques described in [5]. In contrast to the line ratio technique, this approach does not come along with the need of computational expensive collisional-radiative-models (CRMs) and is not limited by the low emission intensity of the 728 nm He I line. It is used to trace single filaments in the SOL as well as high frequency modes with typically 10-100 kHz, which often dominate the dynamics in the confined region close to the separatrix. The evaluation of plasma profiles is done with an advanced dynamic CRM of the helium beam, based on a probabilistic approach, similar to the description in [16].

In this contribution we focus on the plasma edge dynamics of four different scenarios while putting the results into context with other discharges of the same regime. All the discharges are conducted at the same plasma current ($I_p = 800$ kA) and the same central magnetic field $B_t = -2.5$ T. The edge safety factor is therefore very similar for all cases with $q_{95} = 4.8 - 5.3$.

The first example is a low density L-mode discharge (# 36 190, $t = 2-4$ s, $P_{NBI} = 0.6$ MW NBI heating, $n_{core} = 2.7 \times 10^{19}$ m^{-2} line integrated core density, triangularity $\delta = 0.07$). Fig. 1 shows in subplot (a) the n_e and in subplot (b) the T_e profile at the outer plasma edge region. The profiles are time-averaged over a period with constant global plasma parameters. To assess the dynamical behavior on short time scales, the normalized emission of the 587 nm He I line is plotted in subplots (c) – (f) for two different radial positions ($\rho_{pol} = 1$ and $\rho_{pol} = 1.08$, marked with the vertical lines in subplot (a) and (b)) as a function of time. It can be seen that the general turbulence level at the separatrix region is relatively high (noisy appearance of the data) and no large scale structures are formed, as expected for an L-mode discharge [2]. In the far SOL, n_e and T_e and thus the signal base level are low, but interrupted by high intensity bursts, caused by filaments. The statistical analysis of the signal can be found in Section 3.

The second discharge we chose for this comparison is a high density and high triangularity H-mode (# 36 165, $P_{NBI} = 5$ MW, $P_{ECRH} = 2.75$ MW, $n_{core} = 7.5 \times 10^{19}$ m^{-2}, $\delta = 0.27$, see [12, fig. 1] for a time trace of the discharge) with type-I ELMs and small ELMs as defined in [17]. By a step-wise increase in fueling, the ELM amplitude decreases over time, so that after $t = 5$ s no type-I ELMs are left. Before that time point, small ELMs can already be found in inter-type-I ELM phases. The increase in fueling comes along with the formation of a density shoulder [18] (cf. Fig. 2(a)) and Fig. 7, for n_e profiles normalized to the separatrix value), while no significant change is seen in the SOL temperature (see Fig. 2(b)). The rising density during the discharge leads to an increase of filamentary activity (see Section 3), which broadens the power fall-off length as discussed in [12]. Due to the high number of filaments the footprint of single small ELM events cannot be distinguished anymore in the divertor, so that this regime is called quasi continuous exhaust (QCE) regime. Fig. 2 compares the dynamics in the phase with type-I and small ELMs ($t = 2.33-2.33$ s, subplot (c), (d), blue) to the QCE regime ($t = 6.11 - 6.16$ s, subplot (e), (f), red). It can be seen that in the QCE regime the duration of the events (measured by the autocorrelation time τ_a, see Table 1) in both regions, at the separatrix (orange) and far SOL (purple) is smaller compared to the type-I ELM regime, whereas the repetition rate is increased.

The last example chosen for this comparison is an ELM free EDA H-mode scenario (# 36 124, $t = 5 - 5.2$ s, $P_{ECRH} = 1.65$ MW, $n_{core} = 8 \times 10^{19}$ m^{-2}, $\delta = 0.28$). This scenario as described in [19,20], exhibiting several desirable properties for future reactors, such as high density, good energy confinement, possibility of access at low input torque and power, with dominant electron heating, and no impurity accumulation despite the absence of ELMs. The necessary outward transport of impurities in this scenario is supposed to be carried by an increased filamentary activity, which in turn seems to be connected

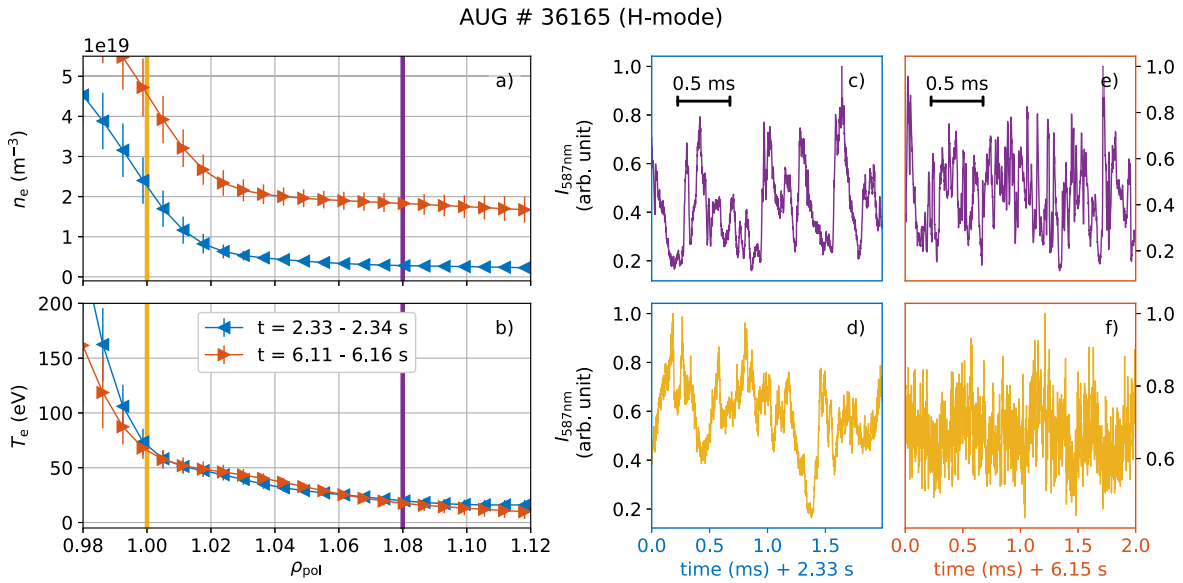

Fig. 2. (a) n_e and (b) T_e plasma profiles for AUG discharge # 36 165. Two time spans are shown for the type-I ELM regime 2.33-2.34 s and the QCE regime 6.11-6.16 s (cf.Fig. 7, for n_e profiles normalized to the separatrix value). Subplots (c) – (f) show the plasma dynamics color-coded at two radial positions $\rho_{pol} = 1$ and $\rho_{pol} = 1.08$, marked by vertical lines in subplots (a) and (b), for two 2 ms long time-spans, respectively.

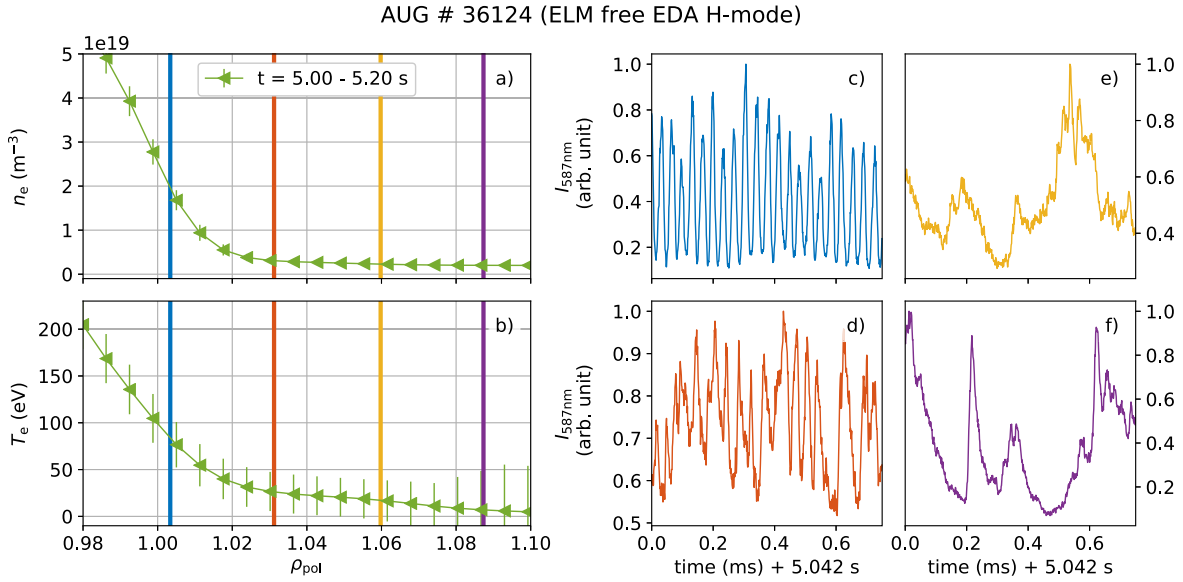

Fig. 3. (a) n_e and (b) T_e plasma profiles for the ELM free EDA H-mode discharge # 36 124. Subplots (c) – (f) show the plasma dynamics color-coded at different radial positions marked by vertical lines in subplots (a) and (b).

to the presence of a strong mode at the separatrix region. This strong edge quasi-coherent mode is always present in these ELM free EDA scenarios and likely plays a key role in maintaining a stationary ELM-free pedestal [20]. The pronounced mode with a frequency of 29 kHz can directly be seen in the THB raw signal around the separatrix position as illustrated in time trace c) of Fig. 3. Furthermore, Fig. 3, shows three additional time traces at different radial positions of the plasma, each with the same window length of 0.75 ms. Whereas the direct influence of the mode is still visible at $\rho_{pol} = 1.03$, the duration of events in the far SOL is increased compared to the mode wavelength and the dynamics is given by intermittent filaments with an occurrence rate of 1.4 kHz.

Figs. 1 to 3 are connecting the plasma dynamics at selected radial positions to averaged n_e and T_e values. To illustrate the fluctuation dynamics over the complete plasma edge region Fig. 4 is introduced. It shows the relative emission change along the plasma radius as a function of time. The time windows of 20 ms length show the L-mode in subplot (a), the type-I ELMy H-mode in subplot (c) and the QCE regime in subplot (d). The window length for the ELM free EDA H-mode in subplot (b) is chosen to be 2 ms, so that the pronounced high frequency mode at the separatrix can be seen directly. The separatrix position is given by the white line, separating the SOL at the top (increasing radius) and the confined region at the bottom.

The H-mode in Fig. 4(c) shows two pronounced type-I ELMs which influence the magnetic equilibrium and expel a significant amount of particles and energy into the SOL. In contrast to that, the QCE regime does not show large scale structures as the whole SOL is filled with frequent fast moving filaments.

To reveal the existence of high frequency modes which are not as coherent as in the ELM free EDA case, a Fourier based spectral analysis of the signal in the confined region close to the separatrix is shown in Fig. 5. Subplots (a) and (d) show broad features around

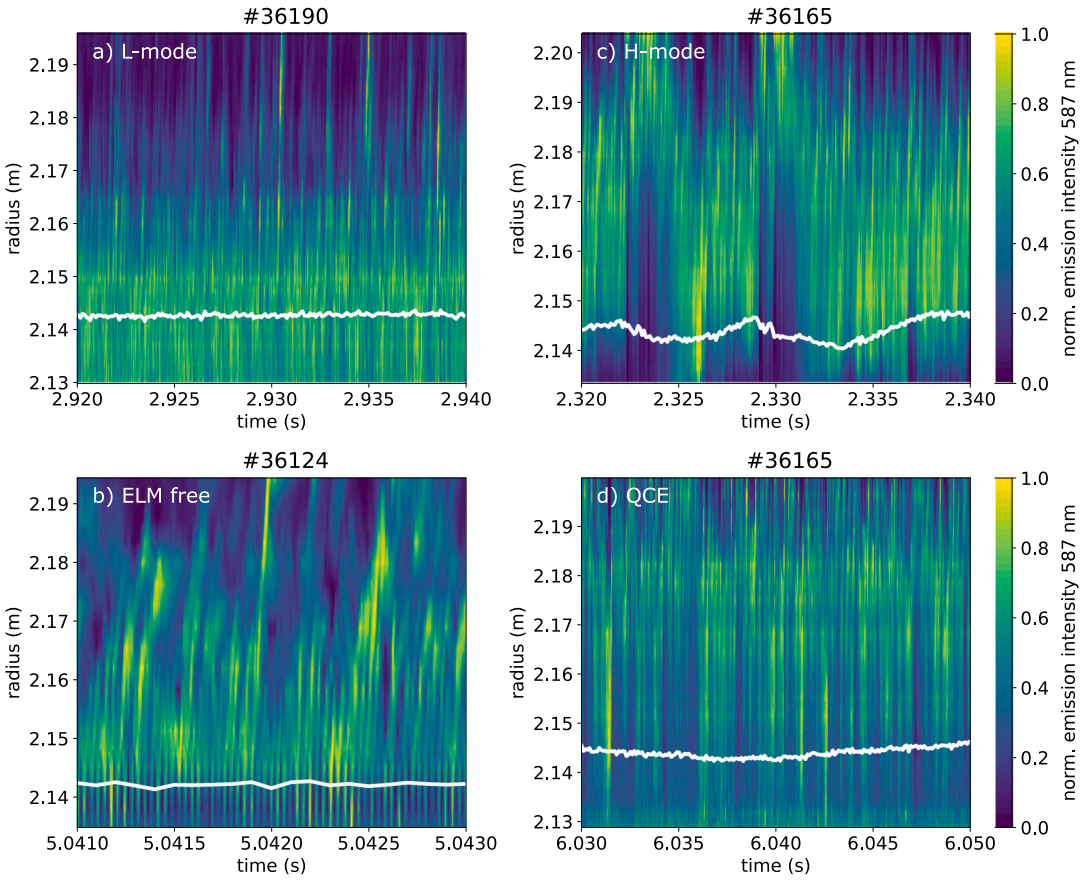

Fig. 4. Normalized helium emission as a function of plasma radius and time. The white line as separatrix position separates the SOL at the top from the confined region at the bottom. The subplots show 20 ms time windows for an L-mode (a), H-mode (c) and the QCE regime (d). For the ELM free EDA scenario (b) a time window of only 2 ms is chosen to present the high frequency mode.

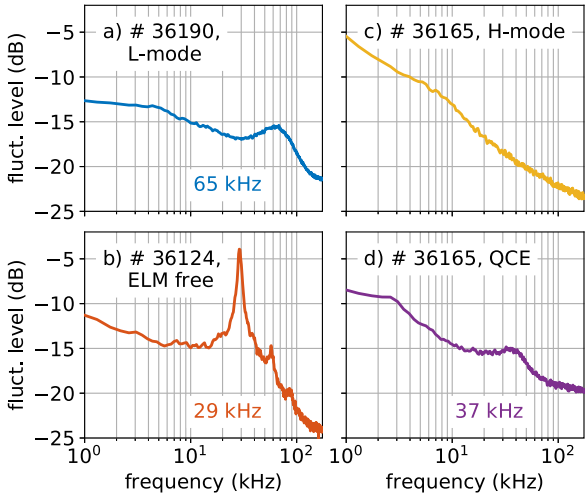

Fig. 5. Frequency spectra of the THB signal at the separatrix for different scenarios. (a) shows an L-mode (# 36 190 $t = 2 - 4$ s), (b) an ELM free EDA H-mode (# 36 124 $t = 5.0 - 5.2$ s), (c) a high density H-mode with small and type-I ELMs (# 36 165 $t = 2.2 - 2.7$ s) and (d) the QCE scenario (# 36 165 $t = 6.1 - 6.6$ s).

65 kHz and 37 kHz, respectively, whereas in the H-mode (subplot (c)), no pronounced mode is present. The broad band in L-mode and the QCE regime is also visible in channels further in the confined region where a change in the dominant frequency towards lower frequencies can be observed. For the L-mode case in Fig. 5(a), for example, the frequency changes from 60 kHz at $\rho_{\mathrm{pol}} = 0.99$ to 65 kHz at the separatrix.

Because the measured mode frequency is dominated by the structure of the mode (n, m) and the local radial electric field strength, the radial change of the mode frequency indicates the existence of several different modes in this region. In contrast, the coherent mode with 29 kHz in the ELM free EDA regime (subplot (b)) is visible in all channels with the same frequency. It is therefore not possible to accurately localize this mode.

3. Filament properties

Table 1 gives an overview of the plasma edge dynamics presented in Section 2, supplemented with two additional discharges; an L-mode with higher density as well as a lower n_e H-mode with clear type-I ELMs and no small ELMs. For filament detection, a 2.5σ criterion is applied on the emission signals of the 587 nm He I line at a position of $\rho_{\mathrm{pol}} = 1.08$. The third standardized moment $\tilde{\mu}_{3,\mathrm{SOL}}$ as a measure of skewness as well as the autocorrelation time are calculated from the same emission time traces. As calculated with a 2.5σ criterion, the filament frequency is not assumed to be constant in the SOL, but depends on the background levels of n_e and T_e. Furthermore the plasma equilibrium (shape, closeness to double null, local connection length and limiter shadowing) influences the filament behavior and detection rates. To show these differences, Table 1 includes the filament frequency at $\rho_{\mathrm{pol}} = 1.08$ and the frequency at the outermost channel $f_{\mathrm{fil,out}}$, with a fixed position in real-space. The corresponding value of ρ_{pol} is given in the table as well. A detailed disentanglement of the single influence factors, however, is subject of further investigations.

In Fig. 6 we show a histogram of radial filament velocity distributions for different regimes, as filaments at one certain radial position and confinement scenario show different velocities. For increasing the

Table 1
Summary of selected plasma fluctuation properties for different confinement regimes with varying densities given by the Greenwald fraction n/n_{GW}. $\tilde{\mu}_3$ is the skewness of the 587 nm line emission time trace at the separatrix and SOL at $\rho_{pol} = 1.08$, whereas τ_a is the corresponding autocorrelation time of the signal. $f_{mode,sep}$ is the frequency of quasi-coherent modes at the separatrix position. $v_{r,median,SOL}$ corresponds to the median filament velocity as depicted in Fig. 6. $f_{fil,SOL}$ is the pseudo frequency of filaments at a fixed position of $\rho_{pol} = 1.08$. $f_{fil,out}$ is the filament frequency at the outermost measurement channel, fixed in real-space. The corresponding position in ρ_{pol} is given in the last line.

	L-mode		H-mode			
Characterization	Low n_e	High n_e	Low n_e	High n_e	QCE	ELM free
Shot no. AUG	36 190	34 867	34 867	36 165	36 165	36 124
Time interval (s)	2.0-4.0	1.9-2.5	3.3-5.0	2.2-3.5	6.1-6.6	4.6-5.9
n/n_{GW}	0.28	0.38	0.52	0.73	0.98	0.82
$\tilde{\mu}_{3,sep}$	0.07	0.1	0.35	0.8	1.0	1.1
$\tilde{\mu}_{3,SOL}$	5.0	5.8	0.9	0.7	0.6	1.4
$\tau_{a,sep}$ (μs)	27	135	230	290	49	10
$\tau_{a,SOL}$ (μs)	71	144	270	94	30	64
$f_{mode,sep}$ (kHz)	65	80	–	–	37	29
$v_{r,median,SOL}$ (m/s)	340	360	370	610	1090	580
$f_{fil,SOL}$ (kHz)	0.45	0.32	0.49	0.98	0.7	1.3
$f_{fil,out}$ (kHz)	0.45	0.32	0.56	1.2	1.8	1.2
pos. $f_{fil,out}$ (ρ_{pol})	1.08	1.08	1.1	1.1	1.09	1.09

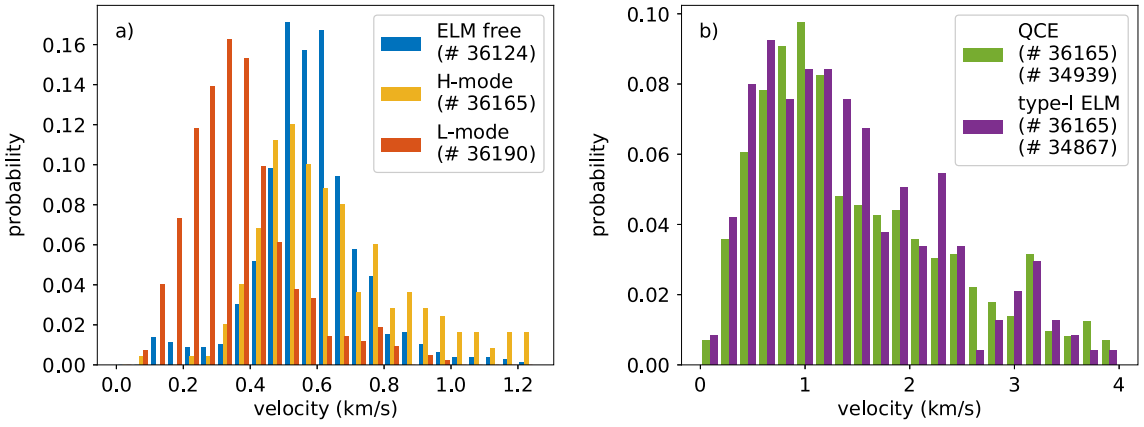

Fig. 6. Comparison of radial filament velocities in the range of $\rho_{pol} = 1.01 - 1.08$. The H-mode scenario # 36 165 ($t = 2.2 - 3.5$ s) is filtered from type-I ELMs, while small ELMs are still contributing to the statistics. The label type-I ELM refers to the ELM filaments themselves.

statistical significance, an additional discharge is added for the QCE regime (# 34 939, $t = 2.5 - 4.5$ s) and the filaments of type-I ELMs (# 34 867, $t = 3.3 - 5$ s), respectively. To simplify the comparison between different regimes, the radial filament velocity is averaged over the radius from $\rho_{pol} = 1.01 - 1.08$, though the measurements confirm a slight deceleration of the radial filament velocity while the filaments propagate outwards as reported in [8].

The analysis shows that frequency and velocity of inter-ELM H-mode filaments are very similar to the typical L-mode case (cf. Table 1, # 34 867, $t = 1.9 - 2.5$ s for L-mode and $t = 3.3 - 5$ s for inter-ELM H-mode), which is in agreement with previous investigations [7,8].

In the high density H-mode (# 36 165, type-I ELMs removed but small ELMs remaining) the radial filament velocity as well as the filament rate are increased compared to the H-mode without small ELMs (# 34 867, $t = 3.3-5$ s). This shows the transition from a turbulence born filament driven transport to an ELM filament driven transport. ELMs or small-ELM like events cause an increase of radial transport by expelling fast filaments into the SOL. The resulting filamentary activity rises in the progress of # 36 165 (cf. [12]). At $t = 6.1 - 6.6$ s, the QCE regime is fully developed and inter-ELM filaments cannot be distinguished from small-ELM filaments. As shown in Fig. 6(b), the filament velocity in the QCE regime (green) is comparable to filament velocities of type-I ELMs (purple). Both are significantly faster than inter-ELM filaments or filaments in L-mode (Fig. 6(a), cf. [9,21]).

The ELM free EDA scenario shows a high filamentary activity like the QCE regime, with nearly the same number of far SOL filaments, but at significantly slower velocities, yet still faster than in L-modes and inter-ELM H-modes.

4. Discussion and conclusion

The L-mode case shows a homogeneous turbulent behavior around the separatrix and near SOL region (corresponding to a low skewness $\tilde{\mu}_{3,sep}$), so that filaments seem to be created from this background turbulence as suggested in [2,10,22]. From there they spread into the far SOL, which subsequently shows a high fluctuation level with a high skewness.

For the ELM free EDA regime and the QCE scenario, filaments dominate the radial plasma edge transport with frequencies around 1 kHz. In the EDA regime, the strong 29 kHz edge mode is likely to drive a frequent filament generation and thus maintains a stationary ELM-free pedestal [20].

In the QCE regime, the high filamentary activity could also possibly be related to the formation of a quasi-coherent mode [23], hypothesized to be of ballooning origin [17]. The mode is not visible at the beginning of discharge # 36 165 (see Fig. 5 c)) and appears first at $t = 3 - 4$ s with a frequency of 53 kHz, sitting at the pedestal bottom. With increased fueling the mode increases in strength and amplitude whereas the frequency decreases to 37 kHz at $t = 6 - 6.2$ s.

A possible picture of filament formation would be that background turbulence or a mode enables transport of particles and energy across

the separatrix. If the plasma conditions allow the formation of interchange modes and thus filaments, the particles in filaments experience charge separation. The resulting $E \times B$ drift velocity of the filament contributes significantly to the overall SOL transport.

A detailed analysis that compares the filament sizes and propagation velocities with the sheath conditions in the divertor or the plasma beta [24] in the filaments is subject of further analysis.

CRediT authorship contribution statement

M. Griener: Conceptualization, Methodology, Software, Formal analysis, Writing - original draft, Writing - review & editing, Visualization. **E. Wolfrum:** Conceptualization, Methodology, Validation. **G. Birkenmeier:** Conceptualization. **M. Faitsch:** Formal analysis. **R. Fischer:** Data curation, Formal analysis. **G. Fuchert:** Formal analysis. **L. Gil:** Formal analysis. **G.F. Harrer:** Validation. **P. Manz:** Conceptualization. **D. Wendler:** Software. **U. Stroth:** Project administration, Funding acquisition. **the ASDEX Upgrade Team:** Funding acquisition. **the EUROfusion MST1 Team:** Funding acquisition.

Declaration of competing interest

The authors declare that they have no known competing financial interests or personal relationships that could have appeared to influence the work reported in this paper.

Acknowledgments

This work has been carried out within the framework of the EUROfusion Consortium and has received funding from the Euratom research and training programme 2014–2018 and 2019–2020 under grant agreement No 633053. The views and opinions expressed herein do not necessarily reflect those of the European Commission. G.F. Harrer is a Fellow of the Friedrich Schiedel Foundationfor Energy Technology.

Appendix

See Fig. 7.

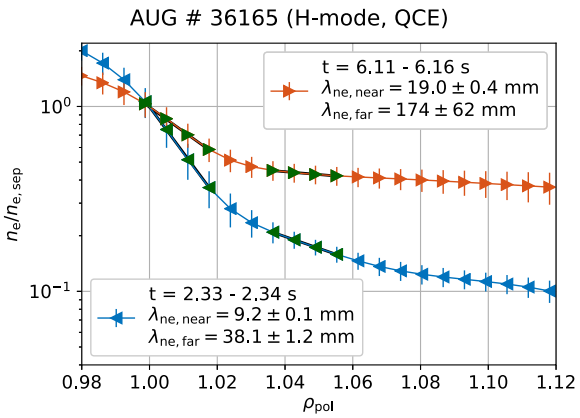

Fig. 7. Electron density (n_e) profiles of AUG H-mode # 36165 (cf. Fig. 2(a)), normalized to the separatrix density $n_{e,sep}$ for two different time points in logarithmic representation. At the later time point the QCE regime and a density shoulder is fully developed as can be seen by comparing the near and far SOL density decay length λ_{ne}. The relevant areas with the exponential fits are highlighted in green.

References

[1] T. Eich, A. Leonard, R. Pitts, W. Fundamenski, R. Goldston, T. Gray, A. Herrmann, A. Kirk, A. Kallenbach, O. Kardaun, A. Kukushkin, B. LaBombard, R. Maingi, M. Makowski, A. Scarabosio, B. Sieglin, J. Terry, A. Thornton, Scaling of the tokamak near the scrape-off layer H-mode power width and implications for ITER, Nucl. Fusion 53 (9) (2013) 093031.

[2] P. Manz, T.T. Ribeiro, B.D. Scott, G. Birkenmeier, D. Carralero, G. Fuchert, S.H. Müller, H.W. Müller, U. Stroth, E. Wolfrum, Origin and turbulence spreading of plasma blobs, Phys. Plasmas 22 (2) (2015) 022308.

[3] S.J. Zweben, J.A. Boedo, O. Grulke, C. Hidalgo, B. LaBombard, R.J. Maqueda, P. Scarin, J.L. Terry, Edge turbulence measurements in toroidal fusion devices, Plasma Phys. Control. Fusion 49 (7) (2007) S1–S23.

[4] A. Theodorsen, O.E. Garcia, Probability distribution functions for intermittent scrape-off layer plasma fluctuations, Plasma Phys. Control. Fusion 60 (3) (2018) 034006.

[5] S.J. Zweben, J. Terry, D. Stotler, R. Maqueda, Invited review article: Gas puff imaging diagnostics of edge plasma turbulence in magnetic fusion devices, Rev. Sci. Instrum. 88 (4) (2017) 41101.

[6] R. Häcker, G. Fuchert, D. Carralero, P. Manz, Estimation of the plasma blob occurrence rate, Phys. Plasmas 25 (1) (2018) 012315.

[7] G. Birkenmeier, F.M. Laggner, M. Willensdorfer, T. Kobayashi, P. Manz, E. Wolfrum, D. Carralero, R. Fischer, B. Sieglin, G. Fuchert, U. Stroth, Magnetic field dependence of the blob dynamics in the edge of ASDEX upgrade L-mode plasmas, Plasma Phys. Control. Fusion 56 (7) (2014) 075019.

[8] G. Fuchert, G. Birkenmeier, D. Carralero, T. Lunt, P. Manz, H.W. Müller, B. Nold, M. Ramisch, V. Rohde, U. Stroth, Blob properties in L- and H-mode from gas-puff imaging in ASDEX upgrade, Plasma Phys. Control. Fusion 56 (12) (2014) 125001.

[9] A. Kirk, H.W. Muller, E. Wolfrum, H. Meyer, A. Herrmann, T. Lunt, V. Rohde, P. Tamain, the MAST and ASDEX Upgrade Team, Comparison of small edge-localized modes on MAST and ASDEX upgrade, Plasma Phys. Control. Fusion 53 (9) (2011) 095008.

[10] D.A. D'Ippolito, J.R. Myra, S.J. Zweben, Convective transport by intermittent blob-filaments: Comparison of theory and experiment, Phys. Plasmas 18 (6) (2011) 060501.

[11] S.J. Zweben, J.R. Myra, W.M. Davis, D.A. D'Ippolito, T.K. Gray, S.M. Kaye, B.P. LeBlanc, R.J. Maqueda, D.A. Russell, D.P. Stotler, Blob structure and motion in the edge and SOL of NSTX, Plasma Phys. Control. Fusion 58 (4) (2016) 044007.

[12] M. Faitsch, T. Eich, G. Harrer, E. Wolfrum, D. Brida, P. David, M. Griener, U. Stroth, Broadening of the power fall-off length in a high density, high confinement H-mode regime in ASDEX upgrade, Nucl. Mater. Energy (2020) submitted for publication.

[13] M. Griener, E. Wolfrum, M. Cavedon, R. Dux, V. Rohde, M. Sochor, J.M. Muñoz Burgos, O. Schmitz, U. Stroth, Helium line ratio spectroscopy for high spatiotemporal resolution plasma edge profile measurements at ASDEX upgrade (invited), Rev. Sci. Instrum. 89 (10) (2018) 10D102.

[14] M. Griener, J.M. Muñoz-Burgos, M. Cavedon, G. Birkenmeier, R. Dux, B. Kurzan, O. Schmitz, B. Sieglin, U. Stroth, E. Viezzer, E. Wolfrum, Qualification and implementation of line ratio spectroscopy on helium as plasma edge diagnostic at ASDEX upgrade, Plasma Phys. Control. Fusion 60 (2) (2018) 025008.

[15] J. Muñoz Burgos, M. Griener, J. Loreau, A. Gorbunov, T. Lunt, O. Schmitz, E. Wolfrum, Evaluation of emission contributions from charge-exchange between the excited states of deuterium with He+ during diagnostic of thermal helium gas beam injection and laser-induced fluorescence, Phys. Plasmas 26 (6) (2019) 063301.

[16] R. Fischer, E. Wolfrum, J. Schweinzer, Probabilistic lithium beam data analysis, Plasma Phys. Control. Fusion 50 (8) (2008) 085009.

[17] G. Harrer, E. Wolfrum, M. Dunne, P. Manz, M. Cavedon, P. Lang, B. Kurzan, T. Eich, B. Labit, J. Stober, H. Meyer, M. Bernert, F. Laggner, F. Aumayr, Parameter dependences of small edge localized modes (ELMs), Nucl. Fusion 58 (11) (2018) 112001.

[18] D. Carralero, S. Artene, M. Bernert, G. Birkenmeier, M. Faitsch, P. Manz, P. de Marne, U. Stroth, M. Wischmeier, E. Wolfrum, On the role of filaments in perpendicular heat transport at the scrape-off layer, Nucl. Fusion 58 (9) (2018) 096015.

[19] M. Greenwald, R. Boivin, P. Bonoli, R. Budny, C. Fiore, J. Goetz, R. Granetz, A. Hubbard, I. Hutchinson, J. Irby, B. LaBombard, Y. Lin, B. Lipschultz, E. Marmar, A. Mazurenko, D. Mossessian, T. Sunn Pedersen, C.S. Pitcher, M. Porkolab, J. Rice, W. Rowan, J. Snipes, G. Schilling, Y. Takase, J. Terry, S. Wolfe, J. Weaver, B. Welch, S. Wukitch, Characterization of enhanced Dα high-confinement modes in Alcator C-Mod, Phys. Plasmas 6 (5) (1999) 1943–1949.

[20] L. Gil, C. Silva, T. Happel, G. Birkenmeier, G. Conway, L. Guimarais, A. Kallenbach, T. Pütterich, J. Santos, P. Schneider, M. Schubert, E. Seliunin, A. Silva, J. Stober, U. Stroth, E. Trier, E. Wolfrum, Stationary ELM-free H-mode in ASDEX upgrade, Nucl. Fusion 60 (5) (2020) 054003.

[21] A. Schmid, A. Herrmann, H. Müller, Experimental observation of the radial propagation of ELM induced filaments on ASDEX upgrade, Plasma Phys. Control. Fusion 50 (4) (2008) 045007.

[22] B. Nold, P. Manz, T.T. Ribeiro, G. Fuchert, G. Birkenmeier, H.W. Müller, M. Ramisch, B.D. Scott, U. Stroth, Turbulent transport across shear layers in magnetically confined plasmas, Phys. Plasmas 21 (10) (2014) 102304.

[23] E. Wolfrum, M. Bernert, J.E. Boom, A. Burckhart, I.G.J. Classen, G.D. Conway, T. Eich, R. Fischer, A. Gude, A. Herrmann, N.C. Luhmann, M. Maraschek, R. McDermott, H.K. Park, T. Pütterich, J. Vicente, B. Wieland, M. Willensdorfer, Characterization of edge profiles and fluctuations in discharges with type-II and nitrogen-mitigated edge localized modes in ASDEX upgrade, Plasma Phys. Control. Fusion 53 (8) (2011) 085026.

[24] P. Manz, D. Carralero, G. Birkenmeier, H.W. Müller, S.H. Müller, G. Fuchert, B.D. Scott, U. Stroth, Filament velocity scaling laws for warm ions, Phys. Plasmas 20 (10) (2013) 102307.